Supplemental Material

for

The Western Gulf of Corinth (Greece) 2020-2021 seismic crisis and cascading events: first results from the Corinth Rift Laboratory network

Authors: George Kaviris[*1], Panagiotis Elias[2], Vasilis Kapetanidis[1], Anna Serpetsidaki[3], Andreas Karakonstantis[1], Vladimír Plicka[4], Louis De Barros[5], Efthimios Sokos[3], Ioannis Kassaras[1], Vassilis Sakkas[1], Ioannis Spingos[1], Sophie Lambotte[6], Clara Duverger[7], Olivier Lengliné[6], Christos Evangelidis[8], Ioannis Fountoulakis[8], Olga-Joan Ktenidou[8], František Gallovič[4], Simon Bufféral[9], Emilie Klein[9], Aissaoui El Madani[10], Oona Scotti[11], Helene Lyon-Caen[9], Alexis Rigo[9], Panayotis Papadimitriou[1], Nicholas Voulgaris[1], Jiri Zahradnik[4], Anne Deschamps[5], Pierre Briole[9], Pascal Bernard[10]

[*]Corresponding Author: gkaviris@geol.uoa.gr

Affiliations:

[1] Section of Geophysics-Geothermics, Department of Geology and Geoenvironment, National and Kapodistrian University of Athens, Greece

[2] Institute for Astronomy, Astrophysics, Space Applications and Remote Sensing, National Observatory of Athens

[3] Seismological Laboratory, Department of Geology, University of Patras, Greece

[4] Faculty of Mathematics and Physics, Charles University, Czech Republic

[5] Université Côte d'Azur, CNRS, Observatoire de la Côte d'Azur, IRD, Géoazur, France

[6] EOST, ITES, Université de Strasbourg, CNRS, France

[7] Commissariat à l'énergie atomique et aux énergies alternatives, DAM, DIF, France

[8] Institute of Geodynamics, National Observatory of Athens, Greece

[9] Laboratoire de Géologie, CNRS, École Normale Supérieure, PSL University, France

[10] Équipe de Sismologie, Institut de Physique du Globe de Paris, France

[11] Bureau d'Évaluation des Risques Sismiques pour la Sûreté des Installations, IRSN, France

Table of Contents

Section S1: Moment tensor inversion additional information

The Moment Tensor (MT) inversion was performed for the five strongest events (M_w = 4.5-5.3) of the sequence (Table S1). The ISOLA platform (Sokos and Zahradnik, 2008; Zahradnik and Sokos, 2018) was employed. Complete waveforms were used, without separating individual phases. Full-wave Green's functions were calculated by the discrete wavenumber method in a 1D velocity model (Rigo et al., 1996). MTs were calculated by the least-squares method. The centroid depths are grid-searched below epicenters. The results are expressed in terms of the double-couple component of the deviatoric solution, represented by the scalar moment, strike, dip and rake. The variance reduction, which quantifies the observed/synthetic waveforms fit for a moment tensor solution, is considered to indicate a good fit when it is larger than 60%, whereas uncertainty factors were also checked (Fig. S1). The results were cross-checked using the first motion polarities of the P-wave arrivals. Both the CRL network and HUSN broad-band stations (ANX, SERG, PDO, AXS, GUR, DRO, PVO, PLEV, LTK, UPR, EVR, LAKA) were involved in the process. The stations are located to the north and south of the Corinth Gulf, at a maximum

epicentral distance of 60 km. Moreover, the results are coherent to the solutions calculated by other seismological institutes (available at EMSC; https://www.emsc-csem.org/).

Table S1. Focal mechanisms solutions for the 5 major events (M_w≥4.5) of the 2020-2021 seismic crisis in the Western Gulf of Corinth. Coordinates and hypocentral (Hypo.) depths are from the location procedure with HypoInverse, whereas centroid depths from the MT inversion procedure. VR: Variance Reduction, # Stat.: Number of stations, CLID: Cluster ID (spatial group number).

Date YYYYMMDD	**Origin** hh:mm	**Lon** (°)	**Lat** (°)	**Hypo. Depth** (km)	**Centroid Depth** (km)	**M_w**	**Seismic Moment** (N·m)	**VR** (%)	**# Stat.**	**Strike** (°)	**Dip** (°)	**Rake** (°)	**CLID**
20201223	14:58	21.990	38.402	9.8	6.0	4.6	8.89E+15	64	6	253	44	-124	1
20210112	22:09	22.038	38.379	6.5	5.5	5.0	4.21E+16	72	8	287	59	-73	2
20210112	22:29	22.044	38.375	8.9	9.5	4.5	7.82E+15	75	8	306	80	-23	2
20210112	22:56	22.045	38.379	8.4	8.5	4.6	9.79E+15	74	8	310	80	-23	2
20210217	03:36	21.940	38.362	7.6	3.5	5.3	1.23E+17	84	8	266	33	-104	3

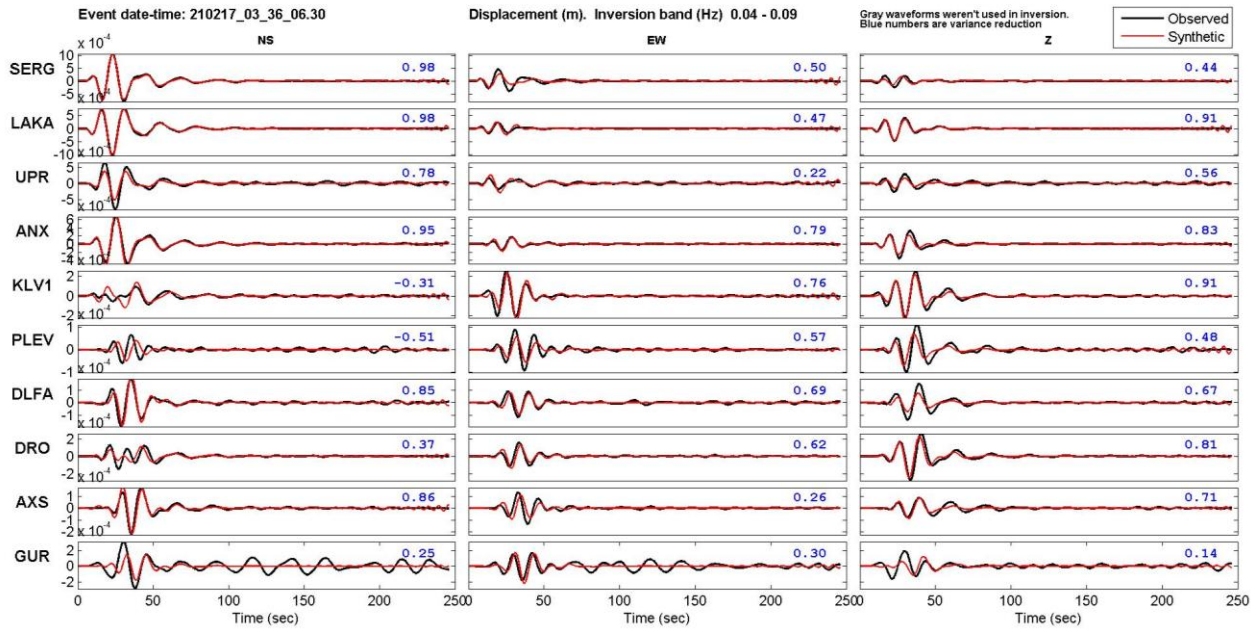

Figure S1. Example of fit between observed (black) and synthetic (red) waveforms yielded by the moment tensor inversion procedure for the 17 February 2021, M_w5.3, mainshock. Values in blue denote the variance reduction for the respective component.

Section S2: Additional tables and figures

Table S2. Observed and modeled displacements at the GNSS stations for the 12 January and 17 February 2021 earthquakes. The uncertainties are ~2 mm for the horizontal and ~6 mm for the vertical displacements, respectively.

Code	Station Coordinates		12 January 2021						17 February 2021					
			Observed			Modeled			Observed			Modeled		
	Long	Lat	dE	dN	dU	dE	dN	dU	dE	dN	dU	dE	dN	dU
	°	°	mm	mm	mm	mm	mm	mm	mm	mm	mm	mm	mm	mm
ARSA	21.8167	38.3011	-1	0		-2	-1		0	-3		0	-1	0
EYPA	21.9284	38.4267	2	0		5	-4		2	11	2	1	10	3
LAMB	21.9732	38.3204	-4	-12		-3	-5		-2	-8	1	0	-2	0
TRIZ	22.0727	38.3654	-10	5	-14	-6	1	-16	1	-1	1	-1	0	0
XILI	21.9118	38.3852	4	-2	-6	3	-1	-2	5	9	14	-3	11	5

Table S3. Finite-fault models obtained by the GNSS modeling. The moment is calculated using the value $\mu = 3 \cdot 10^{10}$ Pa for the crust rigidity. The faulting angles are those determined by moment tensor inversion (Table S1). Fault plane models are presented in Fig. S2.

	Center top of the fault			Angles			Size		Slip	Centroid depth	Moment
	Long	Lat	depth	azimuth	dip	rake	length	width			
	°	°	km	°	°		km	km	mm	km	$*10^{16}$ Nm
Inverted	√	√					√	√	√		
January 12	22.022	38.367	5.0	287	59	-73	9.	3.	249	6.3	20.2
February 17	21.902	38.354	2.0	266	33	-104	4.	2.	579	2.6	13.9

Table S4. Fit residuals of the horizontal displacements for the February 17 earthquake with three different centroid depths.

Station	Observed displacements		Modeled displacements with three values of the centroid depth					
			2.6 km		3.6 km		4.6 km	
	dE	dN	dE	dN	dE	dN	dE	dN
Code	mm	mm	mm	mm	mm	mm	mm	mm
ARSA	0	-3	0	-1	0	-1	0	0
EYPA	2	11	1	10	1	5	0	1
LAMB	-2	-8	0	-2	-2	1	-1	0
TRIZ	1	-1	-1	0	0	0	0	0
XILI	5	9	-3	11	0	2	0	0
r.m.s. (mm)			2.5		3.2		3.7	

Table S5. Uncertainties and other location statistics for the dataset of the present study, overall and per spatial group (C1-C3). Phase numbers (# phases) refer to the usable number of P or S phases with non-zero weight after short-distance weighting (see also Fig. S3f). RMS residuals and location uncertainties are standard uncertainty values reported by HypoInverse.

	All	**C1: Marathias**	**C2: Trizonia**	**C3: Psathopyrgos**
# events	2960	1546	716	532
Mean RMS (s)	0.11	0.11	0.11	0.13
Mean ERH (km)	0.31	0.31	0.31	0.27
Mean ERZ (km)	0.86	0.84	0.83	0.84
Mean Depth (km)	7.87	7.72	8.04	7.41
Median # phases	19	18	19	21
Median gap (°)	91	89	100	82

Figure S2. Projections of the fault plane models (rectangles; Table S3) used for the inversion of slip and seismic moment for the earthquakes of 12 January and 17 February 2021 from GNSS data. GNSS stations are marked by yellow pins.

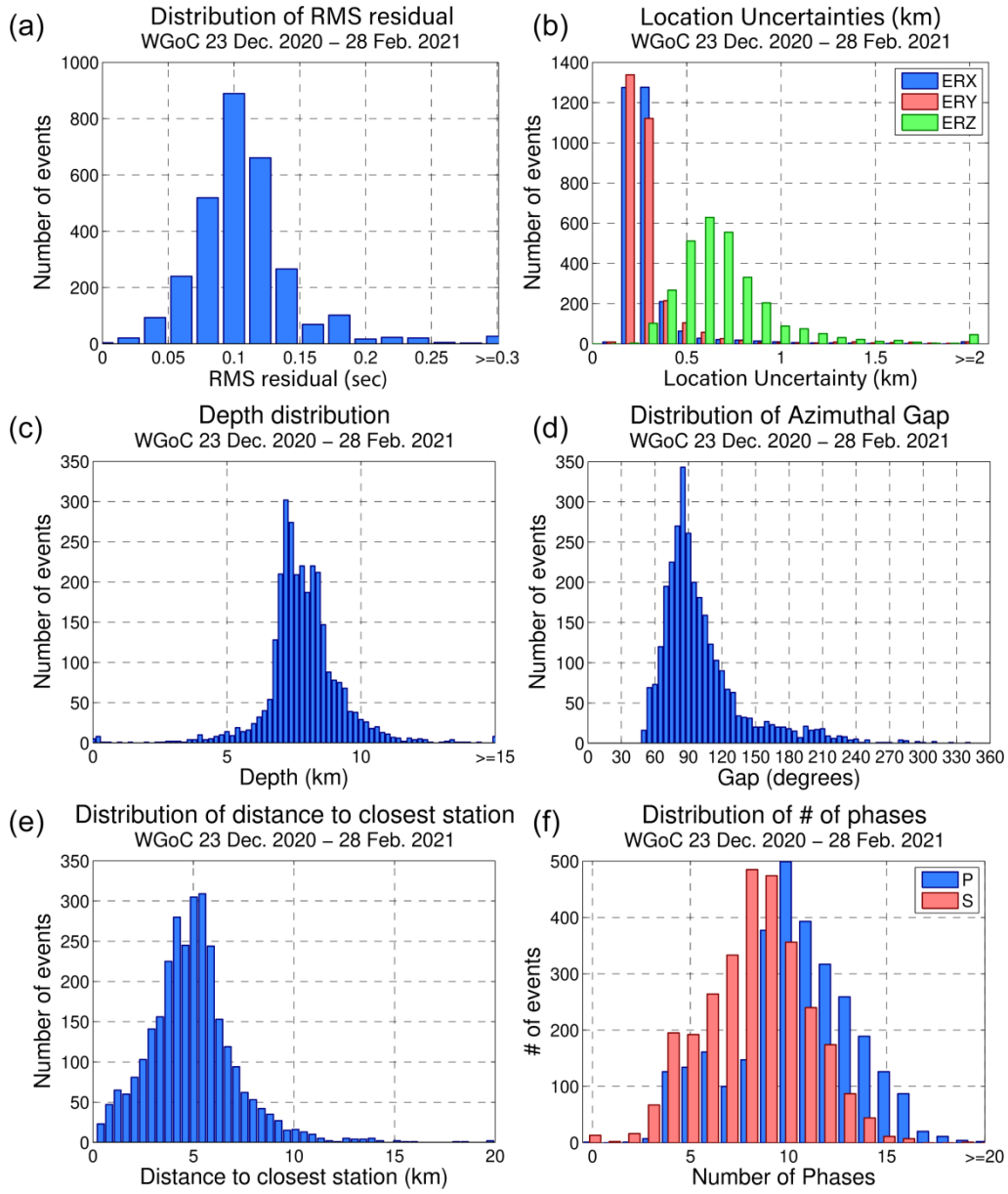

Figure S3. Histograms of location uncertainties (nominal values reported by HypoInverse) and other statistics for the 23 December 2020 – 28 February 2021 seismicity in the WGoC: (a) root-mean-square (RMS) travel-time residuals, (b) horizontal (ERX, ERY) and vertical (ERZ) location uncertainties, (c) focal depths, (d) azimuthal gap, (e) epicentral distance to the closest station with available arrival-time data and (f) number of P- (blue) and S-wave (red) arrival-times with non-zero weight, after the application of short-distance weighting in HypoInverse.

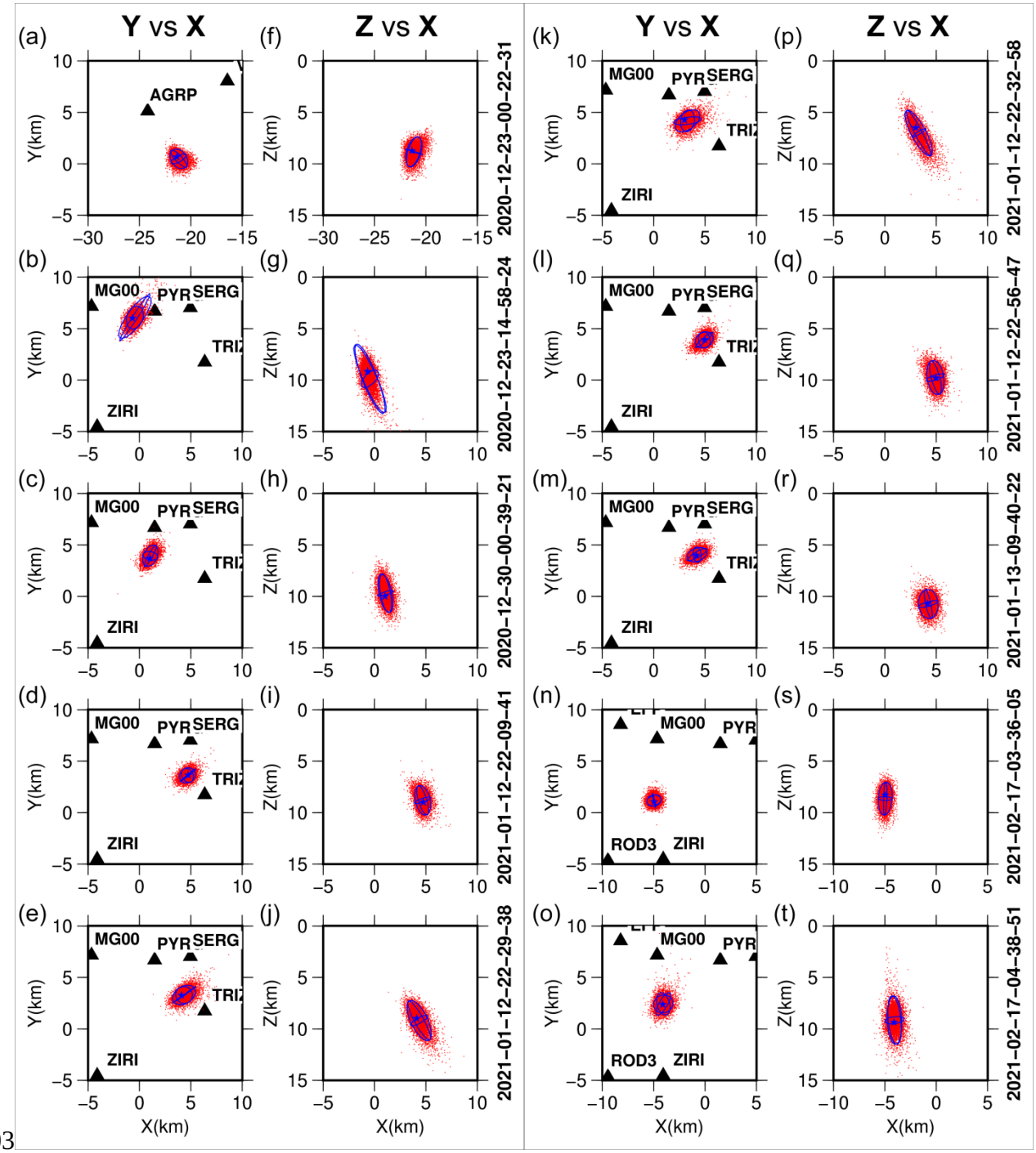

Figure S4. Scatter plots of the probability density function (PDF, red scatter clouds) and the 68% confidence ellipsoid (blue) of the PDF for the 10 stronger earthquakes of the 2020-2021 sequence in the WGoC, determined using the probabilistic Oct-Tree method implemented in the NonLinLoc code (Lomax et al., 2000; http://alomax.free.fr/nlloc/) and the local velocity model

of Rigo et al. (1996). Panels (a-e, k-o) "Y vs X" show a map view of epicenters, whereas panels (f-j, p-t) "Z vs X" represent the depth distribution (Z), with X and Y axes oriented E-W and N-S, respectively. The origin of the horizontal Cartesian coordinates corresponds to Latitude=38.35°N (Y=0) and Longitude=22.00°E (X=0). The resulting uncertainties are ~1 km on the horizontal plane and ~2km in the vertical direction.

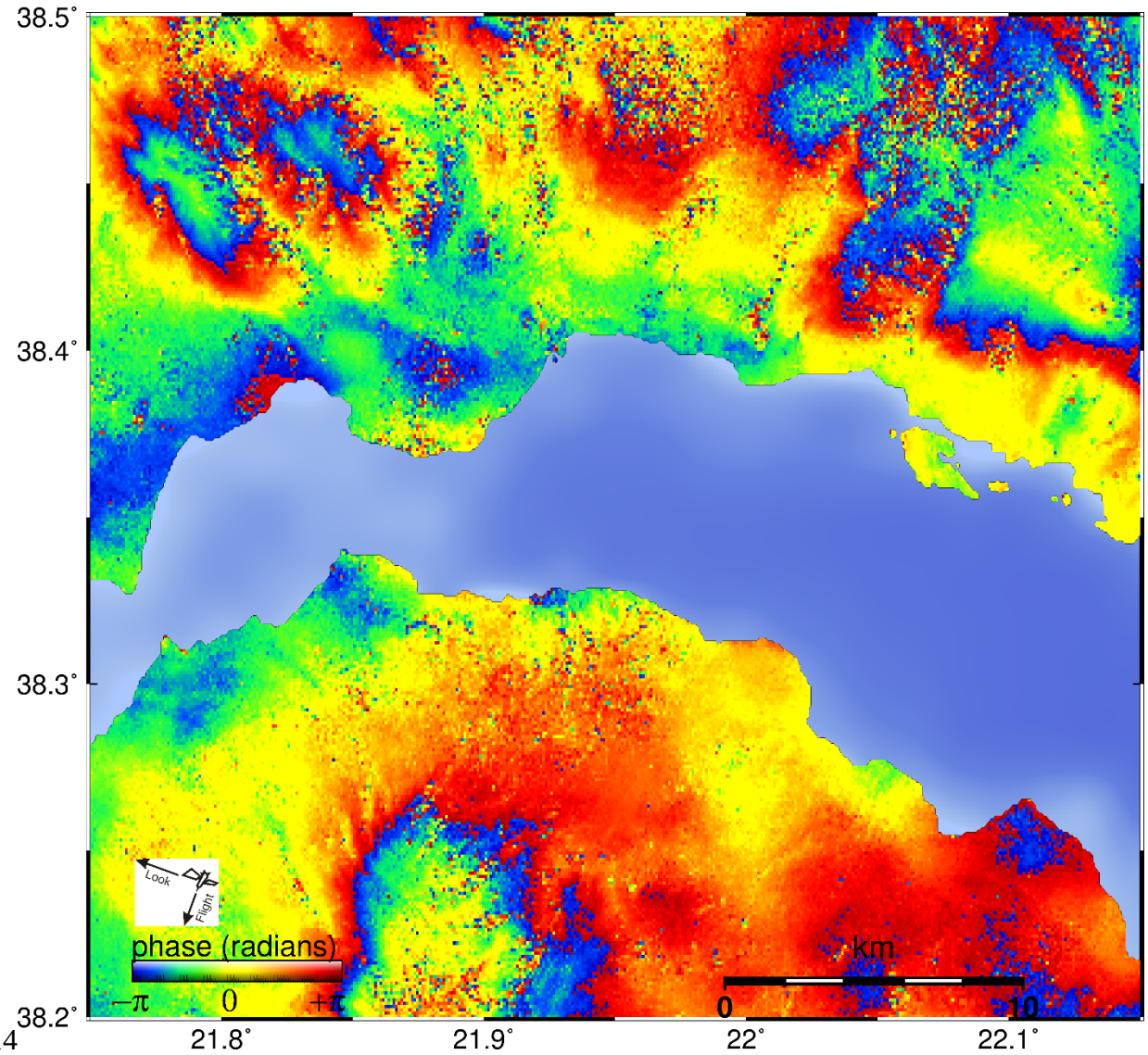

Figure S5. Sentinel-1 interferogram of track 80, in descending orbital geometry, spanning the dates 12/1/2021 and 24/1/2021. No deformation within a quarter of fringe (7 mm) in the line of sight direction is visible.

References

Lomax, A., J. Virieux, P. Volant, and C. Berge-Thierry (2000). Probabilistic Earthquake Location in 3D and Layered Models, in *Advances in Seismic Event Location* C. H. Thurber, and N. Rabinowitz(Editors), Springer Netherlands, Dordrecht, 101–134, doi: 10.1007/978-94-015-9536-0_5.

Rigo, A., H. Lyon-Caen, R. Armijo, A. Deschamps, D. Hatzfeld, K. Makropoulos, P. Papadimitriou, and I. Kassaras (1996). A microseismic study in the western part of the gulf of Corinth (Greece) implication for large-scale normal faulting mechanisms, Geophys. J. Int. 126, 663–688. doi: 10.1111/j.1365-246X.1996.tb04697.x

Sokos, E., and J. Zahradnik (2008). ISOLA-A Fortran code and a Matlab GUI to perform multiple-point source inversion of seismic data, Computers and Geosciences, 34, 967-977. doi: 10.1016/j.cageo.2007.07.005

Zahradník, J., and E. Sokos (2018). ISOLA code for multiple-point source modeling –review. In: “Moment Tensor Solutions - A Useful Tool for Seismotectonics” (S. D'Amico, Ed.), Springer. doi: 10.1007/978-3-319-77359-9_1